Flame aerosol deposition $Y_3Al_5O_{12}:Yb^{3+}$, Er^{3+} nanoparticles on monolayer MoS_2 for broadening near-infrared photoelectroresponse

Haitao Wei[1,2,a],Shuai hu[1,2,b], Tongcheng Yu*[1,2,c]

[1]College of Advanced Interdisciplinary Study, National University of Defense Technology, Changsha, China, 410073

[2]Hunan Provincial Key Laboratory of High Energy Laser Technology, National University of Defense Technology, Changsha, China, 410073

[a] weihaitao0903@nudt.edu.cn, b hushuai0015@163.com, c yutongcheng12@nudt.edu.cn

Abstract. Monolayer molybdenum disulfide (MoS_2) is a two-dimensional material with a direct bandgap widely used in photoelectric detection. It exhibits excellent characteristics such as an ultra-high specific surface area, strong light interaction, and good carrier mobility. However, due to the bandgap limitation, monolayer MoS_2 can only efficiently detect visible wavelengths less than 680 nm. Combining lanthanide-doped upconversion nanoparticles with monolayer MoS_2 to realize near-infrared (NIR) photodetection is a feasible strategy. Thus, $Y_3Al_5O_{12}:Yb^{3+}$, Er^{3+} up-conversion nanoparticles are deposited on the surface of a monolayer MoS_2 by flame aerosol deposition (FAD), significantly extending their photoelectric response range to the near-infrared 980 nm. The $Y_3Al_5O_{12}:Yb^{3+}$, Er^{3+} nanoparticles synthesized by flame can achieve efficient up-conversion from near-infrared (~980 nm) to visible light (~450, ~550, ~650 nm). Therefore, the visible light can be subsequently absorbed by monolayer MoS_2. The carefully designed $Y_3Al_5O_{12}:Yb^{3+}$, Er^{3+}/MoS_2 photodetector shows strong responsivity and highly specific detectivity in the near-infrared spectrum. Under the bias voltage of 3 V and laser irradiation of 980 nm at 2.8 μW, the newly designed MoS_2 device achieves a responsivity of 16.82 A/W and a specific detectivity of 1.47×10^{12} Jones, as the traditional monolayer MoS_2 usually responds to zero. This work can further expand the application of two-dimensional materials and their composites in near-infrared photoelectric detection.

Keywords: Up-conversion nanoparticles, Photoelectric detection, Monolayer MoS_2, Flame aerosol deposition

1. Introduction

Photodetectors are an essential component in the field of information perception, converting optical signals into electrical impulses. The infrared band holds significant importance for photodetectors. By utilizing photoelectric conversion and electrical signal processing to visualize infrared signals that carry the radiation characteristics of objects, infrared photodetectors find wide applications in various fields such as laser radar, night vision imaging, optical fiber communication, and laser distance measurement [1-3].

Two-dimensional materials with atomic layer thickness have been the subject of extensive research recently due to their excellent optical, electrical, and mechanical capabilities [4-9]. Two-dimensional materials, such as black phosphorus (BP) and graphene, have a small or nonexistent intrinsic bandgap, allowing them to achieve a broad-spectrum response, extending up to mid-infrared and terahertz bands [10, 11]. However, the dark current of graphene with zero bandgap is always too high due to the presence of free carriers. The high recombination rate of photogenerated carriers leads to low photoresponse [12]. In addition, black phosphorus has poor stability in the air, making it challenging to realize commercial applications [13, 14].

As a member of the Layered Transition Metal Dichalcogenides (TMDs, MX_2, M= Mo, W, Nb, Ta, Ti, Re; X= S, Se, Te) family, MoS_2 exhibits a strong light-matter interaction, and the band structure is layer (thickness) dependent [15, 16]. The direct bandgap of a monolayer MoS_2 indicates that it could be a promising photoelectric material. However, the carrier mobility of transition metal sulfide is too low, and its detection range is limited to the visible band due to the constraint of bandgap [17].

Combining lanthanide-doped upconversion nanoparticles (UCNPs) on monolayer MoS_2 to realize NIR photodetection is a feasible strategy. The carefully designed UCNPs can couple well with monolayer MoS_2 to achieve the NIR photodetection. Here, Yb^{3+} and Er^{3+} ions are used to realize upconversion from NIR to visible light, and $Y_3Al_5O_{12}$ is selected as the host material for UCNPs due to its low phonon energy and suitability for FAD. For the newly designed $Y_3Al_5O^{12}$: Yb^{3+}, Er^{3+}/MoS_2 hybrid device, $Y_3Al_5O_{12}$: Yb^{3+}, Er^{3+} UCNPs serve as an absorber of near-infrared signals, enabling efficient upconversion from NIR to visible light. MoS_2 works as a receiver of the up-converted radiation energy, realizing the final photoelectric conversion. In summary, we deposited $Y_3Al_5O_{12}$: Yb^{3+}, Er^{3+} UCNPs on monolayer MoS_2 using FAD and achieved a strong photoelectrical response in the NIR.

2. Experimental section

$Y(NO_3)_3$ • $6H_2O$ (99.99%), $Al(NO_3)_3 \cdot 9H_2O$ (99.95%), $Yb(NO_3)_3 \cdot 5H_2O$ (99.99%), $Er(NO_3)_3 \cdot 5H_2O$ (99.99%), n-butanol (98%), and 2-ethylhexanoic acid (2-EHA, >99%) were purchased from Aladdin Industrial Corporation without purification. The MoS_2 flake we utilized was manufactured by SixCarbon Technology Shenzhen. The $Y_3Al_5O_{12}$: Yb^{3+}/Er^{3+} NPs were synthesized using FAD with several modifications [32-34]. The mentioned nitrates were mixed with n-butanol to form the FAD precursor. The molar ratio of rare earth ions (Y^{3+}, Yb^{3+}, Er^{3+}) and Al^{3+} ions in the mixed butanol solution was set at 3:5. Yb^{3+} and Er^{3+} ions constitute 8 % and 1 % of all rare earth elements, respectively. For FAD synthesis, the precursor was subsequently injected into a self-built swirl-stabilized spray flame reactor. A mixture of methane (3 L min^{-1}) and air (30 L min^{-1}) was ignited to create a tubular premixed swirl flame. The spray precursor and air were supplied at rates of 1.2 L h^{-1} and 15 L min^{-1}, respectively, to establish a spray flame for UCNPs synthesis. A water-cooled substrate at the bottom deposits UCNPs above the spray flame. UCNPs will be deposited on a silicon wafer with MoS_2 as the substrate to prepare the $Y_3Al_5O_{12}$: Yb^{3+}, Er^{3+}/MoS_2 hybrid device. Finally, the synthesized UCNPs were calcined in ambient air at 200 ℃ for 2h.

The surface morphologies of the sample were examined by SEM (Hitachi), and PL spectrum were acquired with a lens-coupled grating monochromator (Omnil-l3072i, Zolix) equipped with an integrated photomultiplier tube (PMTH-S1-R928). For photodetection under near-infrared laser, the photocurrent was collected by a semiconductor characterization system (Probe station and Keithley 2612b) under ambient conditions.

3. Results and disscussion

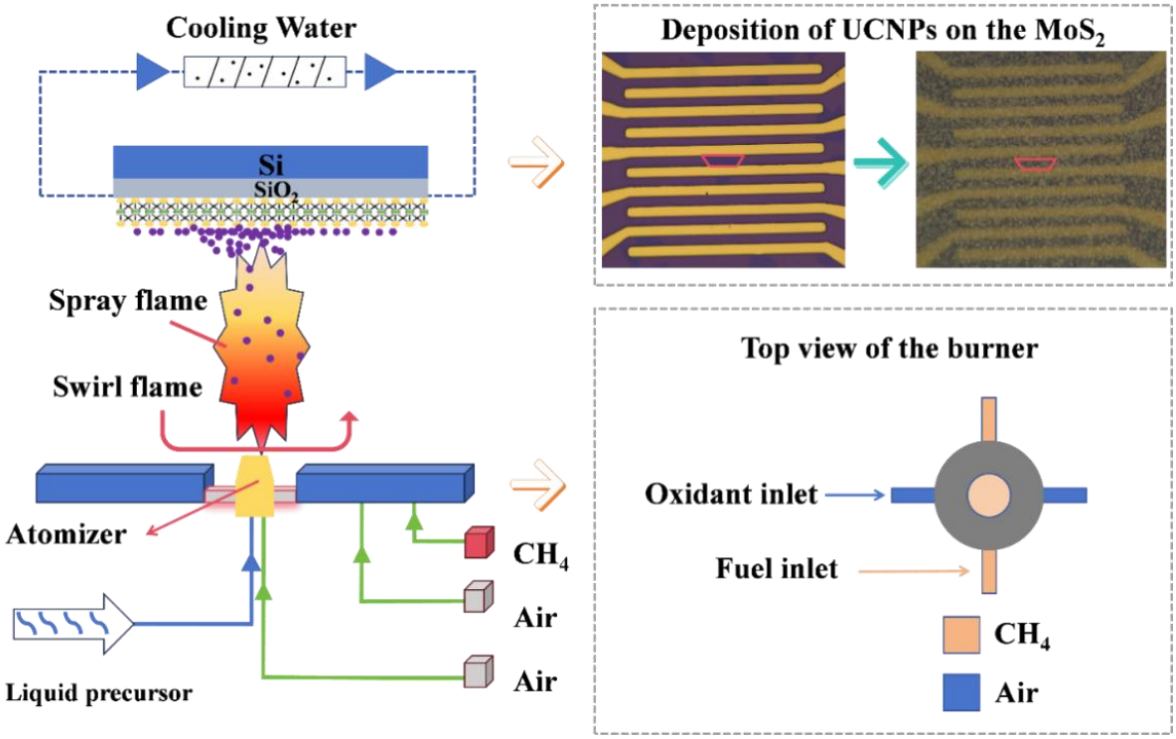

Fig. 1 Schematic illustration of synthesis of $Y_3Al_5O_{12}$: Yb^{3+}, Er^{3+}, which were deposited directly on a silicon wafer with MoS_2.

Fig. 1 depicts the schematic of the synthesis of $Y_3Al_5O_{12}$: Yb^{3+}, Er^{3+} nanoparticles (NPs), which are directly deposited on MoS_2 using silicon wafers as the substrate. This approach is straightforward and efficient, facilitating direct contact between $Y_3Al_5O_{12}$: Yb^{3+}, Er^{3+} NPs and MoS_2. High-temperature annealing is evidently an effective approach to reduce surface defects of NPs, enhancing the efficiency of upconversion luminescence. It is also an important technique for eliminating surface defects in two-dimensional materials and adsorbents to enhance material properties [35]. Our hybrid device has demonstrated high efficiency in photoelectric response under 980 nm laser excitation, achieving a high responsivity of 16.82 A/W and an excellent specific detectivity of 1.47×10^{12} Jones.

Fig. 2(a) displays the cross-sectional image of the hybrid $Y_3Al_5O_{12}$: Yb^{3+}, Er^{3+}/MoS_2 device structure on a SiO_2/Si substrate with Cr/Au contacts and NPs directly attached to the surface of MoS_2. The quality and composition of the MoS_2 and $Y_3Al_5O_{12}$: Yb^{3+}, Er^{3+} UCNPs were studied by Raman spectrum, as shown in Fig 2(b). Based on the interval between E_{2g} and A1g, we inferred that these flakes were monolayer. Fig. 2(c) illustrates a proposed pathway for the energy transfer between $Y_3Al_5O_{12}$: Yb^{3+}, Er^{3+} NPs and MoS_2 flakes. Near-infrared radiation at 980 nm could be absorbed by Yb^{3+}, causing the electrons to transfer from $^2F_7/_2$ to $^2F_5/_2$. The energy is then transferred to Er^{3+}, where high energy levels capture electrons. Radiation of shorter wavelengths (450, 522, 542, 654 nm) is released by the transfer process of $^4F_5/_2$, $^2H_{11}/_2$, $^4S_3/_2$ and $^4F_9/_2 \rightarrow {}^4I_{15}/_2$, which can be absorbed by MoS_2. We then examined the PL spectrum for $Y_3Al_5O_{12}$: Yb^{3+}, Er^{3+} and $Y_3Al_5O_{12}$: Yb^{3+}, Er^{3+}/MoS_2. As demonstrated in Fig. 2(d), $Y_3Al_5O_{12}$: Yb^{3+}, Er^{3+} NPs generate relatively strong fluorescence at 450, 520, 550, 655 nm, which is consistent with the theory. In addition, there is no significant difference in PL spectral intensity between $Y_3Al_5O_{12}$: Yb^{3+}, Er^{3+} and $Y_3Al_5O_{12}$: Yb^{3+}, Er^{3+}/MoS_2. Therefore, we prefer to employ the RET (radiative energy transfer) mechanism to explain the energy transfer between them: $Y_3Al_5O_{12}$: Yb^{3+}, Er^{3+} NPs absorb longer wavelength incident radiation and convert it to shorter wavelength radiation, which is then absorbed by MoS_2.

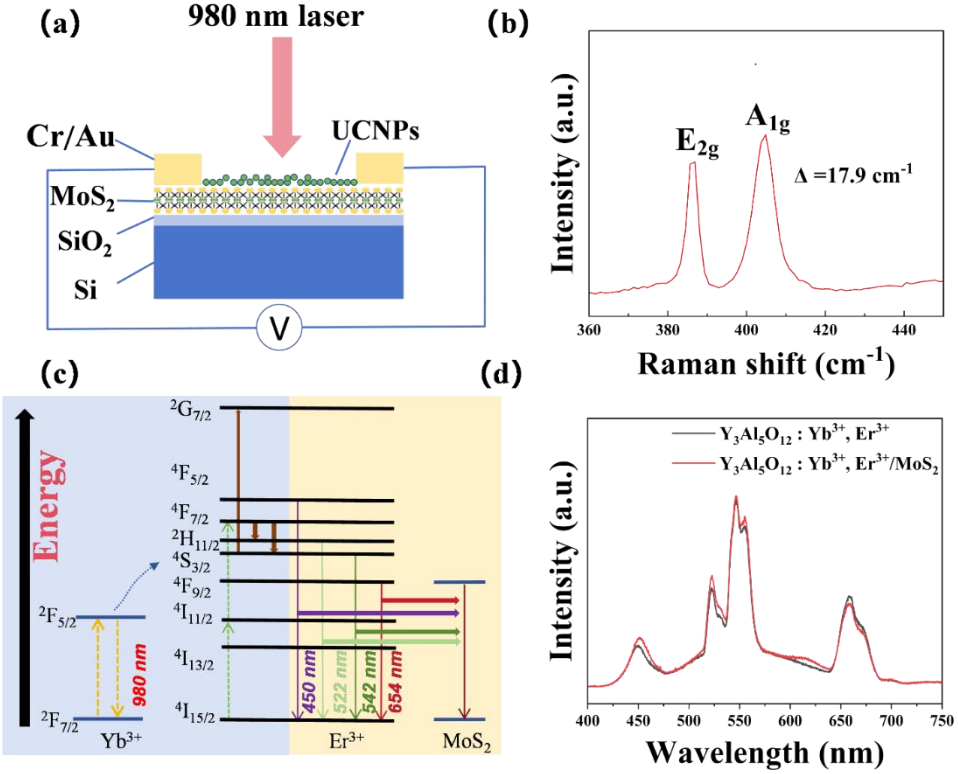

Fig. 2. (a) Schematic diagram of $Y_3Al_5O_{12}$: Yb^{3+}, Er^{3+}/MoS_2 device. (b) Raman spectrum of monolayer MoS_2. (c) Schematic diagram of the excitation of electrons and the energy transfer from $Y_3Al_5O_{12}$: Yb^{3+}, Er^{3+} to MoS_2 in the hybrid device. (d) PL spectrum of bare $Y_3Al_5O_{12}$: Yb^{3+}, Er^{3+}, $Y_3Al_5O_{12}$: Yb^{3+}, Er^{3+}/MoS_2 structure.

The photoresponse of the $Y_3Al_5O_{12}$: Yb^{3+}, Er^{3+}/MoS_2 photodetector is shown in Fig. 3. Fig. 3(a) depicts the photoresponse of a 980 nm laser excitation at different bias voltages of 1 V, 2 V, and 3 V (P = 3.3 mW), and the photoresponse increases noticeably with the increase of V_{ds}. Fig. 3(b) shows

the current-voltage (I-V) characteristic of the $Y_3Al_5O_{12}$: Yb^{3+}, Er^{3+}/MoS_2 hybrid device under varying power 980 nm laser excitation. It can be seen that the Ids increases with the increase of power, and the curve exhibits an obvious symmetry, indicating a good ohmic contact between the electrode and MoS_2 channel. Stable and repeated switching characteristic curves of the $Y_3Al_5O_{12}$: Yb^{3+}, Er^{3+}/MoS_2 hybrid device with a bias of 3V under different power 980 nm laser excitation are shown in Fig. 3(c). In addition, when the laser irradiation strength is increased, the photoresponse of the $Y_3Al_5O_{12}$: Yb^{3+}, Er^{3+}/MoS_2 hybrid device increases. The optimal photoresponse can be achieved by modulating the bias and laser power.

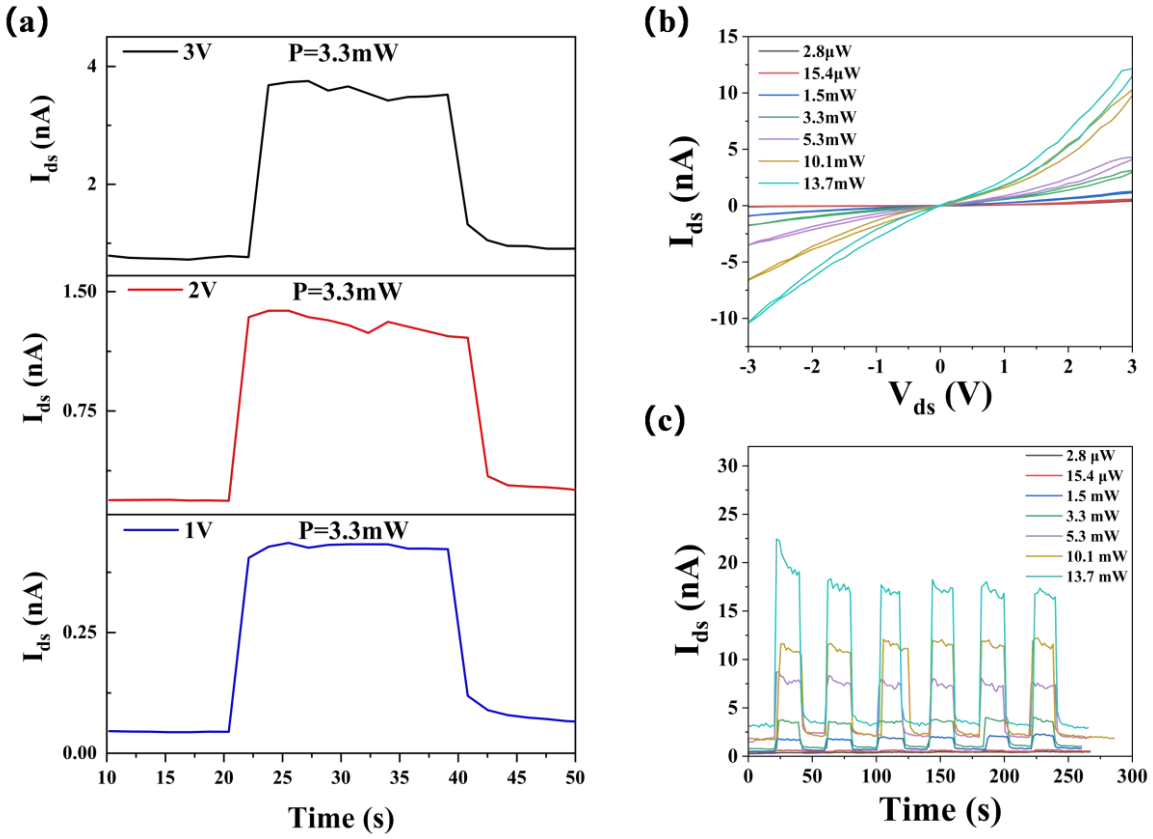

Fig. 3 (a) The photoresponse of 980 nm laser excitation at different bias voltages (P = 3.3 mW).

(b) Current-voltage (I-V) characteristic of the $Y_3Al_5O_{12}$: Yb^{3+}, Er^{3+}/MoS_2 hybrid device under different power 980 nm laser excitation. (c) Stable and repeated switching characteristic curves of $Y_3Al_5O_{12}$: Yb^{3+}, Er^{3+}/MoS_2 hybrid device with a bias of 3 V under different power 980 nm laser excitation.

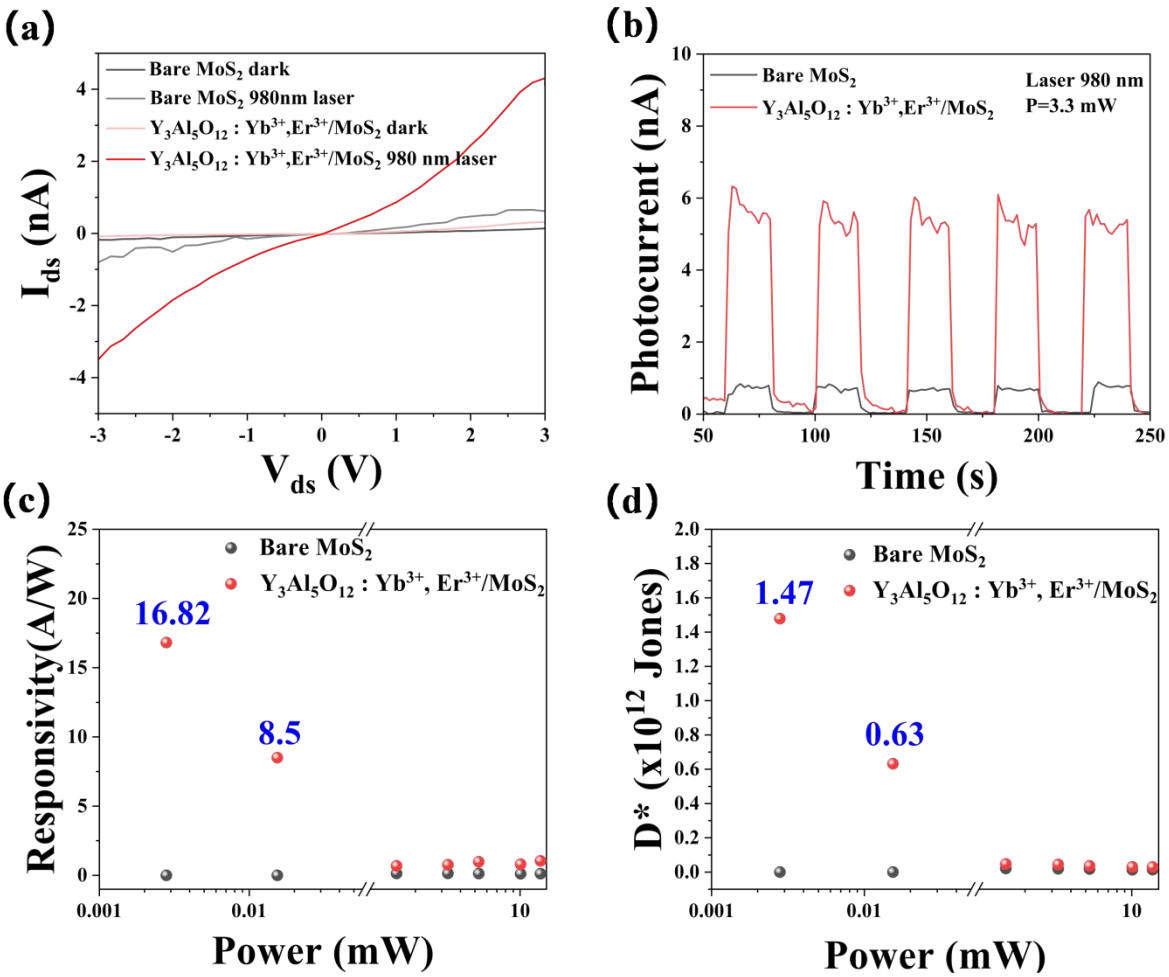

Fig. 4 (a) Current-voltage (I-V) characteristic of both devices, under dark conditions and under illumination with a 980 nm laser. (b) Stable and repeated switching characteristic curves of bare MoS_2 and $Y_3Al_5O_{12}$: Yb^{3+}, Er^{3+}/MoS_2 hybrid device with a bias of 3 V. (c) Responsivity and (d) Specific Detectivity of both devices dependent on intensity of 980 nm laser illumination.

Fig. 4(a) shows the current-voltage (I-V) characteristic of both devices under dark conditions when illuminated by a 980 nm laser. The bare MoS_2 photodetector exhibited an extremely weak photocurrent under 980 nm illumination, which is nearly equal to the dark current. Electrons cannot transit from the valence band to the conduction band because the photon energy provided by the 980 nm laser is less than the band gap energy of monolayer MoS_2. Therefore, the weak response might be caused by the thermal excitation of the laser heating. In addition, the dark current of bare MoS_2 and $Y_3Al_5O_{12}$: Yb^{3+}, Er^{3+}/MoS_2 hybrid device is similar, and the $Y_3Al_5O_{12}$: Yb^{3+}, Er^{3+}/MoS_2 hybrid device showed a strong photocurrent under 980 nm illumination. Fig. 4(b) displays the switching characteristic curves of bare MoS_2 and $Y_3Al_5O_{12}$: Yb^{3+}, Er^{3+}/MoS_2 hybrid device with a bias of 3V. The hybrid device's improved photoresponse is more clearly displayed by the curve. The performance of photodetectors can be evaluated by Responsivity (R) and Specific Detectivity (D*). These parameters can be determined by the following formulas:

$$R = \frac{I_{light} - I_{dark}}{PS} \#(1)$$

$$D^* = \frac{R\sqrt{S}}{\sqrt{2eI_{dark}}} \#(2)$$

where Ilight is the photocurrent, Idark is the dark current, P is the light power, S represents the effective device area, and e is the electron charge.

As shown in Fig. 4(c) and 4(d), the R and D^* of both devices are dependent on the intensity of 980 nm laser illumination. With the increase of laser power, the responsivity and specific detectivity of $Y_3Al_5O_{12}$: Yb^{3+}, Er^{3+}/MoS_2 photodetectors decline. This decline may be caused by photoexcited carriers' recombination due to the adsorbates [42]and the limited upconversion efficiency of $Y_3Al_5O_{12}$: Yb^{3+}, Er^{3+}. Under a laser power of 2.8 μW， the $Y_3Al_5O_{12}$: Yb^{3+}, Er^{3+}/MoS_2 hybrid device achieved a responsivity of 16.82 A/W and a specific detectivity of 1.47×10^{12} Jones, in contrast to the zero response of monolayer MoS_2. Table 1 shows previous studies of similar photodetectors (PDs) included in the study.

Table 1 Previous studies of similar PDs included in the study.

Materials	R(A/W)	D* (x10^{12} Jones)	Wavelength (nm)	Ref
MoS_2/UCMCs	10^{-4}	10^{-4}	980	[36]
Monolayer MoS_2/UCNPs	0.0105	/	980	[37]
Ag NPs- multilayer MoS2	8.81×10^{-4}	1.28×10^{-3}	980	[38]
$Sb2Te_3$	21.7	0.122	980	[39]
$MAPbI_3/CsxWO_3/NaYF_4/NaYF_4$:$Yb^{3+}$, Er^{3+}@NaYF4:Yb^{3+}, Tm^{3+}	0.33	0.045	980	[40]
MoS_2-UCNPs	85	71.4	980	[41]
$Y_3Al_5O_{12}$: Yb^{3+}, Er^{3+}/MoS_2	16.82	1.47	980	This work

4. Conclusion

In summary, we have developed a high-performance $Y_3Al_5O_{12}$: Yb^{3+}, Er^{3+}/MoS_2 photodetector. $Y_3Al_5O_{12}$: Yb^{3+}, Er^{3+} acts as an absorber of near-infrared light, efficiently converting it into visible light. MoS_2 acts as a receiver of the up-converted radiation energy. The photodetector exhibits outstanding performance with an ultrahigh responsivity of up to 16.82 A/W and a large specific detectivity of 1.47×10^{12} Jones when illuminated by a 980 nm laser. Our research provides new

possibilities for designing high-performance two-dimensional optoelectronic devices in the near-infrared spectrum

5. Acknowledgments

We acknowledge the support of Hunan Provincial Key Laboratory of High Energy Laser Technology, National University of Defense Technology, Changsha, China, and the Preresearch Project on Civil Aerospace Technologies funded by China National Space Administration (Grant No. D010105).

Author Contributions

Haitao Wei, Tongcheng Yu performed conceptualization, Haitao Wei, Shuai hu performed investigation and data analysis. Tongcheng Yu supervised the work progress. Haitao Wei wrote the manuscript.

Data Availability Statement

Data is contained within the article or supplementary material. The original contributions presented in the study are included in the article, further inquiries can be directed to the corresponding authors.

Reference

[1] A. Di Bartolomeo, A. Kumar, O. Durante et al. Temperature-dependent photoconductivity in two-dimensional MoS2 transistors. Materials Today Nano, 2023, 24, 100382.

[2] F. Wang, Y. Zhang, Y. Gao et al. 2D metal chalcogenides for IR photodetection. Small, 2019, 15(30), 1901347.

[3] X. Wang, H. Shen, Y. Chen et al. Multimechanism synergistic photodetectors with ultrabroad spectrum response from 375 nm to 10 μm. Advanced Science, 2019, 6(15), 1901050.

[4] Q. Qiu, and Z. Huang. Photodetectors of 2D materials from ultraviolet to terahertz waves. Advanced Materials, 2021, 33(15), 2008126.

[5] D. Jariwala, T. J. Marks, and M. C. Hersam. Mixed-dimensional van der Waals heterostructures. Nature Materials, 2017, 16(2), 170-181.

[6] P. Miró, M. Audiffred, and T. Heine. An atlas of two-dimensional materials, Chemical Society reviews. 2014, 43 18, 6537-54.

[7] Y. Hu, T. Chen, X. Wang et al. Controlled growth and photoconductive properties of hexagonal SnS2 nanoflakes with mesa-shaped atomic steps. Nano Research, 2017, 10(4), 1434-1447.

[8] Y. Hu, L. Mao, X. Yuan et al. Controllable growth and flexible optoelectronic devices of regularly-assembled Bi2S3 semiconductor nanowire bifurcated junctions and crosslinked networks. Nano Research, 2020, 13(8), 2226-2232.

[9] Y. Hu, Z.-H. Qi, J. Lu et al. van der Waals epitaxial growth and interfacial passivation of two-dimensional single-crystalline few-layer gray arsenic nanoflakes. Chemistry of Materials, 2019, 31(12), 4524-4535.

[10] J. Bullock, M. Amani, J. Cho et al. Polarization-resolved black phosphorus/molybdenum disulfide mid-wave infrared photodiodes with high detectivity at room temperature. Nature Photonics, 2018, 12(10), 601-607.

[11] A. Gao, J. Lai, Y. Wang et al. Observation of ballistic avalanche phenomena in nanoscale vertical InSe/BP heterostructures, Nature Nanotechnology, 2019, 14(3), 217-222.

[12] J. D. Buron, F. Pizzocchero, P. U. Jepsen et al. Graphene mobility mapping. Scientific Reports, 2015, 5(1), 12305.

[13] X. Chen, X. Lu, B. Deng et al. Widely tunable black phosphorus mid-infrared photodetector. Nature Communications, 2017, 8(1), 1672.

[14] [14] A. Castellanos-Gomez. Black phosphorus: narrow gap, wide applications. The Journal of Physical Chemistry Letters, 2015, 6(21), 4280-4291.

[15] A. Castellanos-Gomez, M. Barkelid, A. M. Goossens et al. Laser-Thinning of MoS2: on demand generation of a single-layer semiconductor. Nano Letters, 2012, 12(6), 3187-3192.

[16] L. F. Mattheiss. Band structures of transition-metal-dichalcogenide layer compounds, Physical Review B, 1973, 8, 3719-3740.

[17] H. Dong, L. D. Sun, and C. H. Yan. Basic understanding of the lanthanide related upconversion emissions. Nanoscale, 2013, 5(13), 5703-14.

[18] G. Qin, J. Lu, J. F. Bisson et al. Upconversion luminescence of Er3+ in highly transparent YAG ceramics. Solid State Communications, 2004,132(2), 103-106.

[19] S. Hinojosa, O. Barbosa-García, M. A. Meneses-Nava et al. Luminescent properties and energy transfer processes of co-doped Yb–Er poly-crystalline YAG matrix. Optical Materials, 2005, 27(12), 1839-1844.

[20] F. Tang, H. Li, K. Tian et al. Steady-state and time-resolved upconversion photoluminescence in Yb3+-Er3+ co-doped transparent ceramics of YAG. Optics Letters, 2020, 45(20), 5712-5715.

[21] M. Chaika, R. Tomala, O. Vovk et al. Upconversion luminescence in Cr3+: YAG single crystal under infrared excitation. Journal of Luminescence, 2020, 226, 117467.

[22] J. Zhang, S. Wang, T. Rong et al. Upconversion luminescence in Er3+ doped and Yb3+/Er3+ codoped yttria nanocrystalline powders. Journal of the American Ceramic Society, 2004, 87(6), 1072-1075.

[23] T. Tani, L. Mädler, and S. E. Pratsinis. Synthesis of zinc oxide/silica composite nanoparticles by flame spray pyrolysis. Journal of Materials Science, 2002, 37(21), 4627-4632.

[24] A. I. Y. Tok, F. Y. C. Boey, and X. L. Zhao. Novel synthesis of Al2O3 nanoparticles by flame spray pyrolysis. Journal of Materials Processing Technology, 2006, 178(1), 270-273.

[25] S. E. Pratsinis. Aerosol-based technologies in nanoscale manufacturing: from functional materials to devices through core chemical engineering. AIChE Journal, 2010, 56(12), 3028-3035.

[26] S. Li, Y. Ren, P. Biswas et al. Flame aerosol synthesis of nanostructured materials and functional devices: Processing, modeling, and diagnostics. Progress in Energy and Combustion Science, 2016, 55, 1-59.

[27] G. A. Kelesidis, E. Goudeli, and S. E. Pratsinis. Flame synthesis of functional nanostructured materials and devices: Surface growth and aggregation. Proceedings of the Combustion Institute, 2017, 36(1), 29-50.

[28] R. Strobel, and S. E. Pratsinis. Flame aerosol synthesis of smart nanostructured materials. Journal of Materials Chemistry, 2007, 17(45), 4743-4756.

[29] N. Sakar, H. Gergeroglu, S. A. Akalin et al. Synthesis, structural and optical characterization of Nd: YAG powders via flame spray pyrolysis. Optical Materials, 2020, 103, 109819.

[30] A. Prnová, A. Plško, J. Valúchová et al. Crystallization kinetics of glass microspheres with yttrium aluminium garnet (YAG) composition. Journal of Thermal Analysis and Calorimetry, 2018, 131(2), 1115-1123.

[31] R. M. Laine, J. Marchal, H. Sun et al. A new Y3Al5O12 phase produced by liquid-feed flame spray pyrolysis (LF-FSP). Advanced Materials, 2005, 17(7), 830-833.

[32] S. Hu, M. Yuan, L. Wang et al. Aerosol flame synthesis and manipulating upconversion luminescence of ultrasmall Y2O3:Yb3+/Ho3+ nanoparticles. IEEE Photonics Journal, 2022, 14(2), 1-10.

[33] X. Yang, Z. Wu, Z. Yang et al. Flame-made Y2O3:Yb3+/Er3+ upconversion nanoparticles: Mass production synthesis, multicolor tuning and thermal sensing studies. Journal of Alloys and Compounds, 2021, 854, 157078.

[34] S. Hu, M. Yuan, H. Huang et al. Effect of Ce dopant on upconversion and temperature sensing performances in homogeneous ultrasmall Y2O3:Yb3+/Ho3+ nanoparticles through flame aerosol synthesis. Ceramics International, 2023, 49(7), 10953-10960.

[35] X. Zhang, C. Deng, T. Yu et al. Ultraclean surface restoration and giant photoresponse enhancement of violet phosphorus. Applied Surface Science, 2024, 651, 159232.

[36] Y. Zhang, J. Wang, B. Wang et al. Extending the spectral responsivity of MoS2 phototransistors by incorporating up-conversion microcrystals Advanced Optical Materials, 2018, 6(21), 1800660.

[37] N. Zhou, B. Xu, L. Gan et al. Narrowband spectrally selective near-infrared photodetector based on up-conversion nanoparticles used in a 2D hybrid device. Journal of Materials Chemistry C, 2017, 5(7), 1591-1595.

[38] M. J. Park, K. Park, and H. Ko. Near-infrared photodetector achieved by chemically-exfoliated multilayered MoS2 flakes. Applied Surface Science, 2018, 448, 64-70.

[39] K. Zheng, L.-B. Luo, T.-F. Zhang et al. Optoelectronic characteristics of a near infrared light photodetector based on a topological insulator Sb2Te3 film. Journal of Materials Chemistry C, 2015, 3(35), 9154-9160.

[40] Y. Ji, W. Xu, D. Li et al. Semiconductor plasmon enhanced monolayer upconversion nanoparticles for high performance narrowband near-infrared photodetection. Nano Energy, 2019, 61, 211-220.

[41] S. Ghosh, W. C. Chiang, M. Y. Fakhri et al. Ultrasensitive broadband photodetector using electrostatically conjugated MoS2-upconversion nanoparticle nanocomposite Nano Energy, 2020, 67, 104258.

[42] W. Zhang, J.-K. Huang, C.-H. Chen et al. High-gain phototransistors based on a CVD MoS2 monolayer. Advanced Materials, 2013, 25(25), 3456-3461.